THE PUBLISHING HOUSE
OF THE ROMANIAN ACADEMY

PROCEEDINGS OF THE ROMANIAN ACADEMY, Series A,
Volume 21, Number 3/2020, pp. 253–261

NUMERICAL MODELING OF HEMODYNAMIC HEAT TRANSFER IN HYPERTHERMIA TUMOR ABLATION

Alexandru M. MOREGA[1,2], Alin A. DOBRE[1], Alina M. SANDOIU[1], Mihaela MOREGA[1]

[1] "Politehnica" University of Bucharest, Faculty of Electrical Engineering and the Faculty of Medical Engineering, ROMANIA
[2] Gheorghe Mihoc–Caius Iacob Institute of Statistical Mathematics and Applied Mathematics, Romanian Academy
Corresponding author: Alexandru Mihail MOREGA, E-mail: amm@iem.pub.ro

Abstract. Heat transfer in vascularized tissues is commonly described by the bioheat equation (Pennes), which assumes a continuous heat source/sink distribution to model the contribution of the blood vessels to the heat transfer. However, such an approach may be misleading when larger than the capillaries vessels are present too. Along this line, this paper presents a study concerned with sizing the heat transfer needed for a successful operation in planning the localized radio frequency (RF) hyperthermia ablation of a kidney tumor, where the heat is conveyed through hemodynamic flow in larger size vessels and through the tissue, approximated as saturated porous medium, called here the general heat transfer (GHT) model. The results are compared to those obtained by using the bioheat (BHT) model.

Key words: local RF hyperthermia, ablation, bioheat equation, saturated porous media; numerical simulation; finite element method.

1. INTRODUCTION

When planning for the *radiofrequency* (RF) *localized hyperthermia tumor ablation* (LHTA), besides the precise localization of the region of interest (ROI), at least two factors may play an equally important role: the power level of the exposure, and the duration of the procedure. The exposure time is limited and so is the power level for the success of the procedure with minimal side effects, for instance the overexposure of the neighboring healthy tissue.

Despite its known limitations to account for the directional dependence of the perfusion heat source/sink, the morphology of the vascular system (diameters and lengths of vessels), the transvascular transfer of heat and mass, the heat generation by necrosis, the abrupt variation in material properties, the *bioheat equation* (BHE) [1-3] is commonly accepted to model the heat transfer in perfused tissues. In the attempt to alleviate the difficulties posed by this technique, less precise in identifying the distribution of the temperature field when vessels larger than capillaries are identifiable, more comprehensive approaches were proposed, e.g., models that account for local thermal disequilibria [4], models that account for countercurrent blood flow [5], etc.

In this study, departing from the bioheat model (BHM), we propose a conduction-convection heat transfer approach: the anatomic region of interest (solid tissue perfused by capillaries) is seen as a saturated porous medium that embeds and connects to the local arterial and the venous trees. The matrix (solid phase) of the saturated porous medium and the contained fluid (plasma) are in local thermal equilibrium, i.e., a one-temperature model. It is above the purpose of this study to account for the – mesoscale and microscale – anatomic and physiologic details and functionalities. We keep with the macroscopic (continuous media) assumptions and physics, and the blood flow is described by momentum and mass conservation equations, rather than accounted for through a special, empirical source term in the energy equation, as per the BHM. In larger size vessels (i.e., arteries and veins of different sizes) the momentum conservation law is described by either Navier-Stokes or Stokes equation, depending of the local vasculature. The tissues perfused by capillaries, which connect the arterial and the vein trees, are modeled as saturated porous media, and

Brinkman-Stokes momentum balance is used instead. Mass conservation law is then added to the momentum balance equation to close the model. To see the difference between the homogenization-based approach and the convection-conduction formulation, we consider the electromagnetic field radio frequency (RF) LHTA [6-9] used to extirpate a renal tumor. The mathematical model (PDEs) that describes the outlining physics of the RF-LHA procedure is solved for using the finite element method (FEM). Analytical results (if any) may be difficult to obtain due to the complexity of the computational domain (even when using CAD tools to construct it), the non-linearity of the flow equations, and the couplings between the electric field (the heat source that it produces), the hemodynamic flow (heat sink) and the energy equation (in the GHT model).

The structure, vasculature and functioning of the kidney is complex [10-14], some of its functions are still not fully understood, and mathematical models may complement experimental work to clarify this matter [15]. They are affordable, non-invasive yet accurate tools for thought experiments and studies focused on patient-specific parameter selection, design of the electrode [16], and power level. For example, the power may be tuned to ensure a localized overheating of the tumor, thus minimizing unnecessary destruction of the surrounding healthy tissue.

In this study the kidney and the tumor are modeled as saturated porous media [17, 18]. In depth information on porous media flow and heat and averaging techniques, parametrisation of perfusion models is available in [19, 20]. The time scales of the three problems suggest stationary forms for the electric field and the hemodynamic flow, and the dynamic heat transfer [21]. During the procedure the fluids mass flow rates balance are satisfactorily well approximated by the overall inlet to outlet blood mass flows rates balance only. The results are analyzed to unveil the underlying mechanisms and optimization paths of RF-LHA procedures.

2. THE MATHEMATICAL MODEL

The computational domain is CAD generated, Fig. 1 [21], but more realistic, patient-related domains may be constructed using rendering techniques based on medical imagery data sets (e.g., DICOM sets) [22, 23], with spatial resolutions consistent with the continuous media assumptions and the related physics. The number of bifurcations, the lengths and diameters sizes and ratios of the "mother"/"daughters" vessels are consistent with the constructal law predictions [24, 25], in agreement with the allometric laws [26, 27]. The arterial tree segment here is assumed to belong to the entry-level resistance vessels group, Fig. 1 [21]. The alternative, equivalent lumped parameters circuit representation of the kidney hemodynamic, e.g. [28], may result in ordinary differential equations mathematical models that do not provide for the spatial distribution needed in predicting the RF-LHTA.

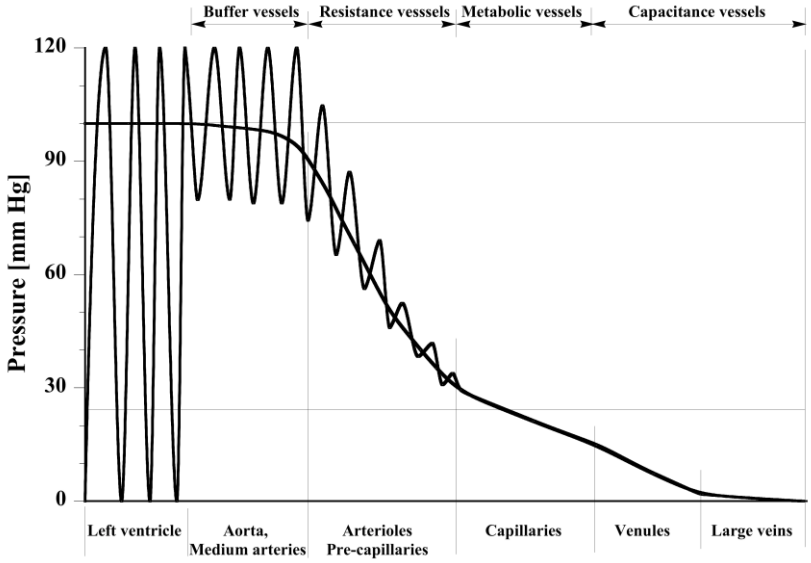

Fig. 1 – Different types of blood vessels.

Although each kidney may be irrigated by up to six arteries, they may receive a single (the renal) artery too [29]. The conceptual study here assumes that the renal artery splits into two arteries prior to supply the kidney, the upper (UD) and lower (LD) divisions, respectively [30]. These, in turn, split into two smaller arteries (Fig. 2). Moreover, the kidney main functions are filtering of the blood and long-term regulation of arterial pressure [31]. The arterial unfiltered blood eventually enters the *nephrons* and reaches the *glomeruli* where the toxins are collected into the *tubules* to be drained out by urine [12, 13, 32]. Filtered blood returns to the bloodstream via the venous system. The entire content of circulatory system (~5 l for an adult) is filtered, typically, every 30 to 60 minutes in humans, depending on the subjects resting heart rate. The RF-LHA procedure lasts maybe ~10 min, while ~ 1 l of blood is filtered, and ~ 0.01 l of urine is produced. Based on these, in this study we neglect the filtering function of the kidney and the oxygen transport [32-35], whose time scale is significantly larger than that of the RF-LHA procedure, and the fluid loss through urine generation and flow.

The RF antenna is a LeVeen array of electrodes by using a trocar guide-way (Fig. 2b,c,d) [36], positioned closely to the tumor by using online imaging techniques (e.g., unenhanced CT) [9]. The tumor volume is embedded in a region prone to its genesis and angiogenesis [37, 38]. The arterial and venous trees constructs mimic the natural morphology. The computational domain may be constructed using CAD tools [38, 39].

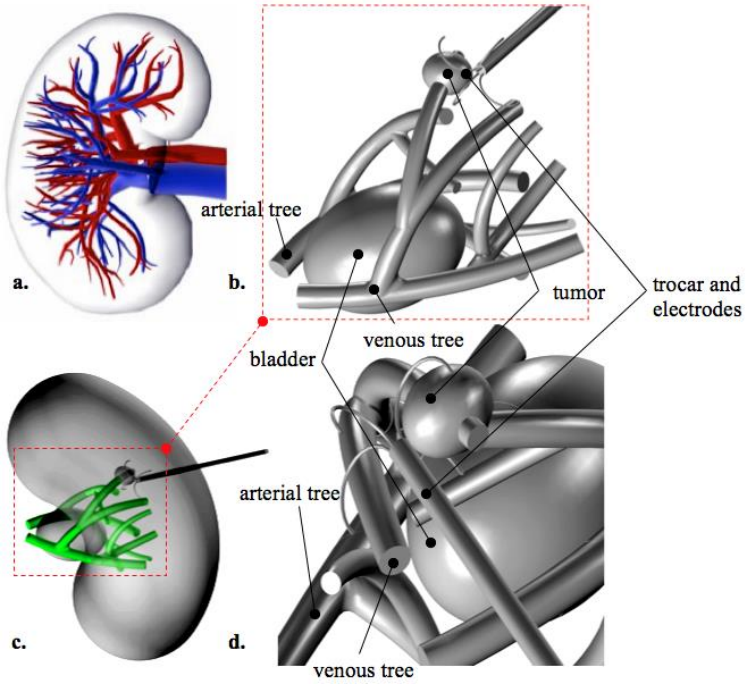

Fig. 2 – The computational domain: (a) conceptual design [3], and (b)–(d) its CAD abstraction.

The *electrokinetic* problem is presented through

$$\nabla \cdot \left(-\sigma \nabla V \right) = 0 \,, \tag{1}$$

where σ is the electrical conductivity (Table 1), and V is the electric potential.

Dirichlet boundary conditions (BCs), Fig. 3, left, are set for the kidney surface (ground) and for the electrode tips (here, $V = 22$ V). In this monopolar, multiple electrode arrangement [36], the current "flows" out of the electrodes tips through the kidney to the body surface, which is connected to the return (ground) electrode. The FEM solution to (1) provides for the electric current density, which may be used to compute the heat source (Joule effect).

Because the kidney hemodynamic is rather slow (Re << 1), we assume a Stokes-type flow inside the porous medium, whereas for the larger vessels (in the arterial and venal trees), where Re ~ $O(10^2)$, Navier-Stokes momentum equation is utilized. Moreover, the flow time scale (~ seconds) is small when compared to

the heat transfer time scale (~ minutes) hence we assume stationary forms of the momentum conservation for larger vessels (Navier-Stokes flow) and porous medium (Brinkman-Stokes flow), respectively

$$\rho\left[(\mathbf{u}\cdot\nabla)\mathbf{u}\right] = -p\mathbf{I} + \mu\left(\nabla\mathbf{u} + (\nabla\mathbf{u})^{\mathrm{T}}\right), \tag{2}$$

$$\nabla\cdot\left[-p\mathbf{I} + \mu\frac{1}{\varepsilon_p}\left(\nabla\mathbf{u} + (\nabla\mathbf{u})^{\mathrm{T}}\right)\right] - \left(\mu\kappa^{-1} + \beta_F|\mathbf{u}| + \frac{Q_{br}}{\varepsilon_p^2}\right) - p\mathbf{I} + \mu\frac{1}{\varepsilon_p}\left(\nabla\mathbf{u} + (\nabla\mathbf{u})^{T}\right)\mathbf{u} = 0, \tag{3}$$

and the mass conservation law (incompressible flow)

$$\rho\nabla\cdot\mathbf{u} = Q_{br}. \tag{4}$$

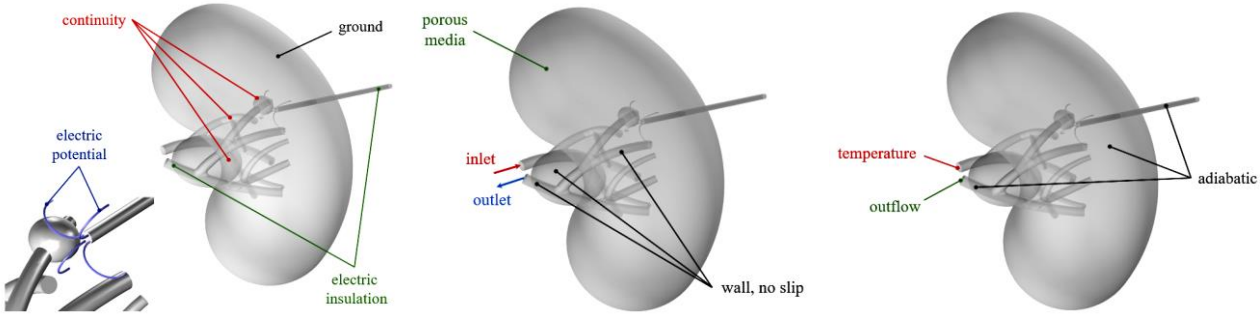

Fig. 3 – Boundary conditions for: the electrokinetic field (left), the hemodynamic (central) and heat transfer (right) problems. The inlet arterial velocity (uniform profile) is 0.1 m/s and uniform pressure profile (0 Pa) is set for the vein outlet (central).

Here $\mathbf{u}$ is the velocity field, p the pressure field, ρ the mass density, μ the dynamic viscosity, $(\cdot)^{\mathrm{T}}$ the transposition operator, $\mathbf{I}$ the unity matrix, κ the permeability, ε_p the porosity, Q_{br} is a mass source (zero here), and β_F is a Forchheimer drag coefficient (zero here). The BCs that close the hemodynamic flow problem related to the GHT model are illustrated in Fig. 3, center.

For the vascular ramification level (kidney) it is suggested to use a non-Newtonian rheological model for the blood. Here we use a power law model, where the dynamic viscosity is $\eta = m\cdot\dot{\gamma}^{n-1}$ and where $m = 0.017$ Pa·s^n (fluid consistency coefficient), $n = 0.708$ (flow behavior index) are model-related parameters, and $\dot{\gamma} = 0.01$ s^{-1} is the lower shear rate limit [22, 41]. For consistency, the flow rate related to the inlet velocity (0.1 m/s) in the GHT model is sized to match the perfusion rate, ω, which has to be set for the BHT model (Table 1). A study aimed to find then consistent values for the permeability and porosity, not presented here, suggests $\kappa = 10^{-9}$ m^2 [42] and $\varepsilon_p = 0.03$. The BCs are presented in Fig. 3, center.

The heat transfer is described by the energy equation

$$\rho C\left[\frac{\partial T}{\partial t} + (\mathbf{u}\cdot\nabla)T\right] = \nabla(k\nabla T) + q, \tag{5}$$

where C is the specific heat capacity at constant pressure (different for porous and fluid media, respectively), T the temperature, k the thermal conductivity (different for porous and fluid media), $q = \rho\mathbf{J}^2$ [W/m^3] is the external heat source (produced by the electric field), and $\mathbf{J} = -\sigma\nabla V$ [A/m^2] is the electric current density. The basal metabolic heat generation rate is neglected here. The arterial blood inlet temperature is set to 37°C, and the surface of the kidney is assumed in thermal equilibrium with its surroundings throughout the numerical simulation, i.e., adiabatic (Fig. 3, right). The validity of this condition is checked against the surface temperature that, for consistency, has to remain at 37°C throughout the simulation time.

Consistent with the BHM, the kidney may be seen as a homogeneous medium with a distributed heat either source or sink that accounts where heat transfer is described through

$$\rho C_p\frac{\partial T}{\partial t} = \nabla(k\nabla T) + \rho_b C_{p,b}\omega(T_b - T) + q. \tag{6}$$

The input parameters, Table 1, are assumed constant for the working conditions. The basal metabolic heat rate is neglected here. In both models, GHT and BHT, only the enlarged part of the *ureter*, the renal pelvis (its upper, large, end-part comprising the *calyces*, cuplike extensions), is considered here. This cavity collects the urine before it flows into the urinary bladder.

Table 1

Electrical, thermal and flow properties [18, 19, 41-45]

Property	**Value**
Basal temperature, T_a	37°C
Blood perfusion rate, ω (in BHT model)	$3.4 \cdot 10^{-3}$ s^{-1}
Dynamic viscosity of blood, μ	5 Pa·s
Electric conductivity of trocar, σ_t	$4 \cdot 10^6$ S/m
Electric conductivity of electrode, σ_e	$1 \cdot 10^8$ S/m
Electric conductivity of blood, σ_b	0.667 S/m
Electric conductivity of urine, σ_u	0.025 S/m
Electric conductivity of kidney and tumor, σ	0.22 S/m
Mass density of blood, ρ_b	1000 kg/m^3
Mass density of kidney and tumor, ρ_t	1080 kg/m^3
Mass density of urine, ρ_u	1000 kg/m^3
Specific heat capacity of blood, $C_{p,b}$	4180 J/(kg·K)
Specific heat capacity of kidney and tumor, C_p	3771 J/(kg·K)
Specific heat capacity of urine, C_u	750 J/(kg·K)
Thermal conductivity of blood, k_b	0.534 W/(m·K)
Thermal conductivity of kidney and tumor, k	0.4182 W/(m·K)
Thermal conductivity of urine, k_u	0.6 W/(m·K)

The volume of fluid contained here does not change throughout the RF-LHA procedure, and it is stagnant. It contributes though to the heat transfer process, and it is modeled as solid volume that may indirectly drain some heat from the ROI under ablation. For the purpose of this study, and consistent with available experimental data, its thermal properties are those of the water [44, 45].

3. NUMERICAL SIMULATION RESULTS

The models (1)-(6) were solved using the finite element method (FEM) [44]. The computational domains are meshed with pyramidal, Lagrange, quadratic elements (Fig. 4).

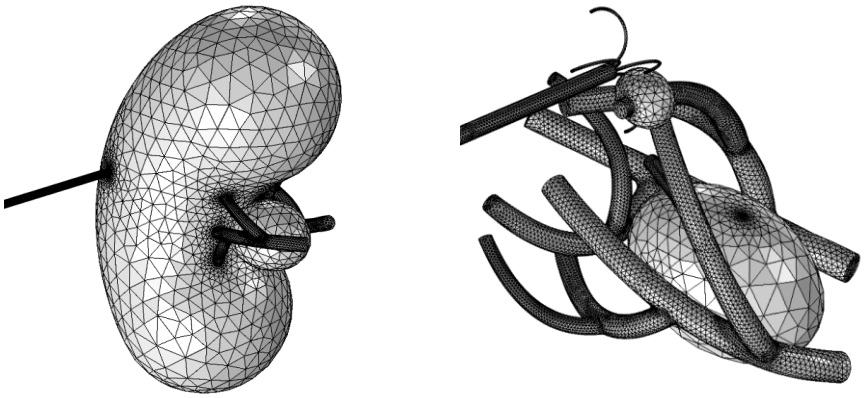

Fig. 4 – The unstructured FEM mesh comprises ~ 450,000 pyramidal elements.

In GHT model, the electrokinetic problem (1) and the hemodynamic (2)-(4) problems are solved in the first place, independently. Next, the dynamic heat transfer PDE (5) is integrated. Figure 6a shows the electrical current driven by the voltage applied at the trocar electrodes. The current path crosses regions with higher electrical conductivity, the blood inside the vessels, to heat them up (by Joule effect). The blood flow

is presented in Fig. 5b,c through the pressure field and the velocity streamlines and proportional arrows. The pressure drop (arterial entrance to the venous exit) is of the order $O(10^4)$, consistent with available experimental data [11, 45]. The arterial flow is connected to the saturated porous medium flow, which in turn is connected to the venous flow.

The procedure may be successful provided the temperature of the targeted tissue is increased to 45°C – the value of the *critical isotherm*. The total (Joule) power received by the tumor is 0.141 W, in the BHT model and 0.149 W in the GHT one. The slight discrepancy may be explained because of the different electrical current density distribution (the electrical conductivities of blood and renal tissue are different).

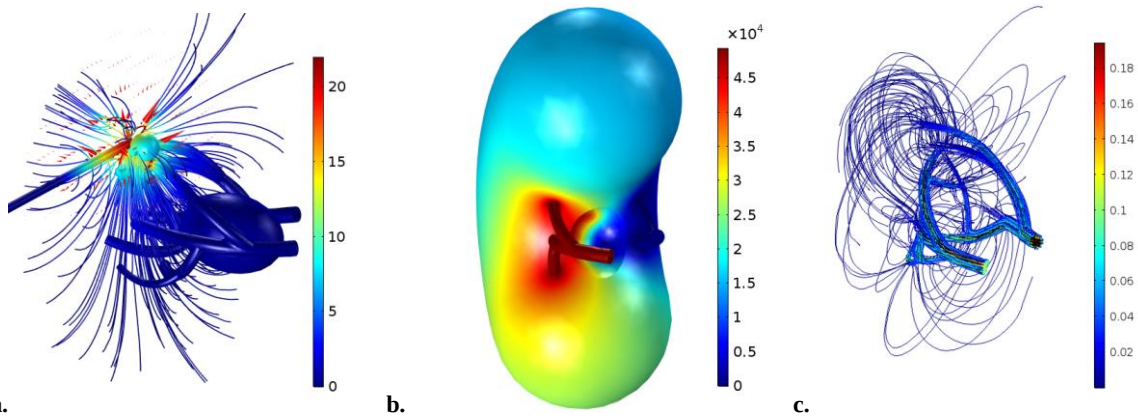

Fig. 5 – Numerical simulation results: a) the electric field inside the kidney trough field lines and arrows for the electric current density; color is proportional to the electric potential (values are in volts); b) the pressure field on the kidney surface (values are in Pa); c) the hemodynamic flow through velocity streamlines and proportional arrows (values are in m/s).

Figure 6 shows this critical isotherm (green), which contains part of the tumor volume after *approx.* 10 min. That region may be thought of as being treated through RF-LHTA. The two models cast different predictions. Whereas the BHM suggests that the tumor is entirely ablated, the general heat transfer model points out that only part of the tumor is well addressed. In both situations, the critical isotherm contains the volume to be ablated, consisting of part of the tumor and also some adjacent, healthy tissue. To reduce the side effects, either better positioning of the electrode array or a second electrode array may be used, but due attention is needed because healthy tissue might also be irreversibly affected.

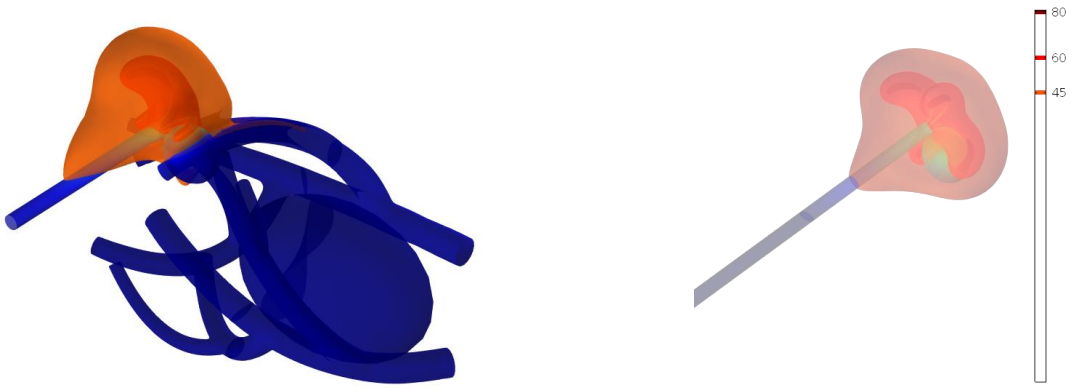

Fig. 6 – The GHT model (left) vs. the BHT model (right): the thermal field in the region of interest after ~10 min, seen through the isotherm of 45°C, which contains the ablated volume, and the 60°C and 80°C inner isotherms. Values are in °C.

Finally, Fig. 7 shows the ROI (tumor) volume-averaged temperature rises to the critical plateau for both models. Perhaps, this is the most important argument that shows the difference between the two models: if numerical simulation is used to aid the planning of the RF-LHTA then the BHT model may be misleading. The temperature predicted by it as promising the success of the planned protocol would be, in fact, highly

overestimated, which would mean a useless intervention – for an invasive procedure such as RF-LHTA this is less good news. Of course, the heating has to be maintained long enough, and a strategy aimed to attain this goal makes the object of a distinct study.

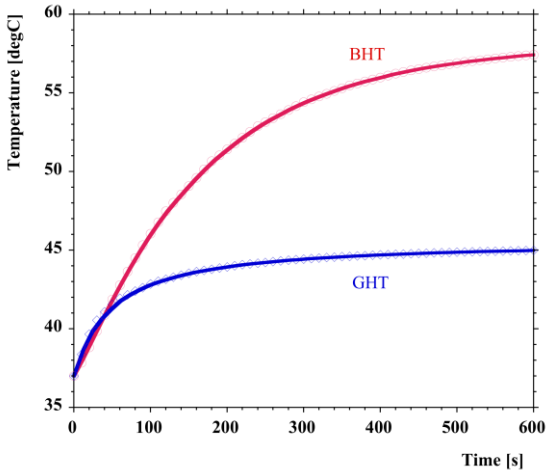

Fig. 7 – The evolution of the volume averaged temperature of the ROI volume (contained by the isotherm of 45°C), which is subject to the hyperthermia ablation.

4. CONCLUSIONS

Radiofrequency localized hyperthermia ablation of tumors (RF-LHTA) is a relatively new, promising, minimum invasive and highly effective tumor extirpation procedure that may be used to eradicate bone, lung, liver, and renal smaller tumors. The heat source is the electro-thermal (Joule) effect. For the success of the LHTA, in the pre-interventional phase aimed at precisely positioning the antenna and adjusting its power, the numerical modeling may complement other medical assertive elements. Although the as simple as possible prediction of operational protocol for localized hyperthermia is the desideratum, the difficulties related to the realistic representation of the targeted tumor volume in the ROI may raise concerns about the accuracy of the numerical modeling when simpler, e.g., homogenization techniques are used.

Along this line, this study presents a comparative analysis of two approaches: the continuous medium, homogenized bioheat (BHM) model, and a continuous medium, general heat transfer (GHT) two-scales model, assuming the kidney is a saturated porous medium (perfused by capillary vessels) that contains arteries and veins, with which it is hemodynamically connected. The larger vessels are identified as significant enthalpy paths that drain part of the power delivered by the electrodes.

It is assumed that a tumor is situated inside the kidney nearby a larger arterial tree. Numerical modeling is conducted on a CAD-drawn domain that mimics the real situation. This numerical experiment is a convenient, cost-efficient tool, useful to understand and plan the procedure to optimally match the patient's specificity.

The two models are consistent in terms of the hemodynamic flow and perfusion rate, size and positioning of ROI and RF antenna. Unlike the BHM, which uses a perfusion term, in the two-scales GHT model the hemodynamic part utilizes the Navier-Stokes (arterial-venous system) momentum balance equation, the Brinkman-Stokes (the renal tissue) momentum balance equation, and the mass conservation equation. Heat transfer by convection and diffusion is presented by the energy equation: a modified form (Pennes equation) for the BHT vs. the general form in the GHT model.

The results unveil the underlying heat generation and transfer mechanisms of this procedure, the hemodynamic of a non-Newtonian fluid (blood), and the local hyperthermia action upon the ROI – the tumor. They clearly evidence the discrepancies between the thermal loads in the two situations (temperature field, power levels, etc.), which suggest that heat transfer through the larger vessels may lead to different predictions hence suggestions for the adequate positioning of the antenna and tuning its power level. This information is particularly important because without this contribution part of the tumor volume might be neglected, whereas the surrounding healthy tissue may be affected to a larger extent.

Finally, although detailed, the computational domain here is build, for convenience, using CAD tools. The reason is that this study is aimed to prove a concept: GHT has to be used instead of the BHT. In fact, for the results to have a patient-related significance, the computational domain should be generated using reconstruction techniques based on the patient's relevant medical scans (DICOM sets), e.g. [22].

This study pleads only for numerical experiments as convenient, cost-efficient, non-invasive tools that may contribute to better understand the RF-LHTA procedure, and find solutions for its optimization.

A future study is concerned with patient-specific, more realistic hyperthermia/ablation analysis. To this end, medical imagery will provide for reconstructed computational domains, e.g. [23]. Furthermore pulsatile blood flow conditions are envisaged.

ACKNOWLEDGEMENTS

The work was conducted in the Laboratory for Electrical Engineering in Medicine, affiliated with BIOINGTEH platform at UPB.

REFERENCES

1. H.H. PENNES, *Analysis of tissue and arterial blood temperature in the resting human forearm*, J. Appl. Phys., **1**, pp. 93-122, 1948.
2. M. SEN, *Bioheat equations – Heat transfer in blood vessels and tissues*, March 17, 2013, https://www.yumpu.com/en/document/view/11525036/bioheat-equations-heat-transfer-in-blood-vessels-and-tissues
3. T.J. VOGL, T.K. HELMBERGER, M.G. MACK, M.F. REISER, *Percutaneous tumor ablation in medical radiology*, Springer-Verlag Berlin Heidelberg, 2008.
4. M.M. CHEN, K.R. HOLMES, *Microvascular contributions in tissue heat transfer*, Annals of the New York Academy of Sciences, **335**, pp. 137-150, 1980.
5. S. WEINBAUM, L.M. JIJI, *A new simplified bioheat equation for the effect of blood flow on local average tissue temperature*, ASME J. of Biomechanical Eng., **107**, pp. 131-139, 1985.
6. E.K. ABDALLA, J.-N. VAUTHEY, L.M. ELLIS, V. ELLIS, R. POLLOCK, K.R. BROGLIO, K. HESS, S.A. CURLEY, *Recurrence and outcomes following hepatic resection, radiofrequency ablation, and combined resection/ablation for colorectal liver metastases*, Annals of Surgery, **239**, *6*, pp. 818-827, June 2004.
7. E.M. KNAVEL, C.L. BRACE, *Tumor ablation: common modalities and general practices*, Tech. Vasc. Interv. Radiol., **16**, *4*, pp. 192-200, 2013.
8. R. RAMANATHAN, R.J. LEVEILLEE, *Ablative therapies for renal tumors*, Ther. Adv. Urol., **2**, *2*, pp. 51-68, 2010.
9. R.J. ZAGORIA, *Imaging-guided radiofrequency ablation of renal masses*, RadioGraphics, **24**, p. 5971, 2004.
10. *Anatomy and Physiology* (3rd edition), pp. 22-28, Text Book Equity, Inc., OpenStax College, Rice Univ., HU, Texas, USA, 2013.
11. A.T. LAYTON, *Mathematical modeling of kidney transport*, Wiley Interdiscip. Rev. Syst. Biol. Med., **5**, *5*, pp. 557-573, September 2013.
12. D.J. MARSH, D.D. POSTNOV, D.J. ROWLAND, A.S. WEXLER, O.V. SOSNOVTSEVA, N.-H. HOLSTEIN-RATHLOU, *Architecture of the rat nephron-arterial network: analysis with micro-computed tomography*, Am. J. Physiol. Renal Physiol., **313**, pp. F351-F360, 2017.
13. D.J. MARSH, D.D. POSTNOV, O.V. SOSNOVTSEVA, N.-H. HOLSTEIN-RATHLOU, *The nephron-arterial network and its interactions*, Am. J. Physiol. Renal Physiol., **316**, pp. F769-F784, May 2019.
14. D.A. NORDSLETTEN, S. BLACKETT, M.D. BENTLEY, E.L. RITMAN, N.P. SMITH, *Structural morphology of renal vasculature*, Am. J. Physiol. Heart Circ. Physiol., **291**, pp. H296-H309, 2006.
15. J.M. SANDS, H.E. LAYTON, *Urine concentrating mechanism and its regulation*, in: *The kidney: physiology and pathophysiology*, 3rd edition, eds. D.W. Seldin, G. Giebisch, pp. 1175-1216, Lippincott Williams and Wilkins, Philadelphia, 2000.
16. M. KODA, S. TOKUNAGA, T. MATONO, T. SUGIHARA, T. NAGAHARA, Y. MURAWAKI, *Comparison between different thickness umbrella-shaped expandable radiofrequency electrodes (SuperSlim and CoAccess): experimental and clinical study*, Experimental and Therapeutic Medicine, **2**, pp. 1215-1220, 2011.
17. G.A. TRUSKEY, F. YUAN, D.F. KATZ, *Transport phenomena in biological systems*, Pearson Prentice Hall, 2004.
18. L. DURLOFSKY, J.F. BRADY, *Analysis of the Brinkman equation as a model for flow in porous media*, Phys. Fluids, **30**, *11*, pp. 3329-3341, 1987.
19. G.A. AMHALHEL, P. FURMAŃSKI, *Problems of modeling flow and heat transfer in porous media*, Institute of Heat Engineering, Biuletyn Instytutu Techniki Cieplnej Politechniki Warszawskiej, **85**, pp. 56-88, 1997.
20. E.R. HYDE, C. MICHLER, J. LEE, A.N. COOKSON, R.C. DAVID, A. NORDSLETTEN, N.P. SMITH, *Parameterisation of multi-scale continuum perfusion models from discrete vascular networks*, Med. Biol. Eng. Comput. **51**, pp. 557-570, 2013.
21. A.A. DOBRE, A.M. MOREGA, L.D. VIRLAN, A.M. SANDOIU, M. MOREGA, *Planning of renal tumor ablation aided by numerical modelling*, Proc. of the 10th International Symposium on Advanced Topics in Electrical Engineering (ATEE 2017), pp. 274-278, Bucharest, Romania, March 23-25, 2017.

22. A.M. MOREGA, A.A. DOBRE, M. MOREGA, *Numerical simulation of magnetic drug targeting with flow structural interaction in an arterial branching region of interest*, Comsol Conf., Versailles, France, November 17-19, 2010.
23. A.M. MOREGA, A.A. DOBRE, M. MOREGA, *Electrical cardiometry simulation for the assessment of circulatory parameters*, Proc. of the Romanian Academy, Series A, **17**, *3*, pp. 259-266, 2016.
24. A. BEJAN, *Shape and structure, from Engineering to Nature*, Cambridge Univ, Press., 2000.
25. A. BEJAN, J.P. ZANE, *Design in nature. How constructal law governs evolution in biology, physics, technology, and social organization*, Anchor Books, Random House Inc. New York, 2012.
26. C.D. MURRAY, *The physiological principle of minimum work: II. Oxygen exchange in capillaries*, Proc. of the National Academy of Sciences of the United States of America, **12**, *5*, pp. 299-304, 1926.
27. C.D. MURRAY, *The physiological principle of minimum work: I. The vascular system and the cost of blood volume*, Proc. of the National Academy of Sciences of the United States of America, **12**, *3*, pp. 207-214, 1926.
28. D.D. POSTNOV, D.J. MARSH, D.E. POSTNOV, T.H. BRAUNSTEIN, N.-H. HOLSTEIN-RATHLOU, E.A. MARTENS, O. SOSNOVTSEVA, *Modeling of kidney hemodynamics: probability-based topology of an arterial network*, PLoS computational biology, **12**, *7*, e1004922, 2016.
29. D. BACHMANN, E. HAASNER, *Truncus Intercosto-renalis. Fortschr. Geb. Rontgenstr. Nuklearmed.*, **102**, pp. 712-713, cited by "Illustrated Encyclopedia of Human Anatomic Variation, Opus II: Cardiovascular system: arteries: thorax intercostal artery", R.A. Bergman, A.K. Afifi, R. Miyauchi, 1965.
30. F.K. WACKER, H. LIPPERT, R. PABST, *Atlas der arteriellen Variationen* (II Bauch und Becken), Chap. 11 "Nierenarterie", A. Renalis, 2018.
31. I. SGOURALIS, R.G. EVANS, B.S. GARDINER, J.A. SMITH, B.C. FRY, A.T. LAYTON, *Renal hemodynamics, function, and oxygenation during cardiac surgery performed on cardiopulmonary bypass: a modeling study*, Physiological Reports, **3**, *1*, e12260, pp. 1-14, 2015.
32. National Institute of Health, National Institute of Diabetes and Digestive and Kidney Diseases, U.S. Department of Health and Human Services, *Your kidneys & how they work*, https://www.niddk.nih.gov/health-information/kidney-disease/kidneys-how-they-work, 2019.
33. B.C. FRY, A. EDWARDS, I. SGOURALIS, A.T. LAYTON, *Impact of renal medullary three-dimensional architecture on oxygen transport*, Am. J. Physiol. Renal Physiol., **307**, *3*, pp. F263-F272, August 2014.
34. C.-J. LEE, B.S. GARDINER, R.G. EVANS, D.W. SMITH, *A model of oxygen transport in the rat renal medulla*, Am. J. Physiol. Renal Physiol., **315**, *6*, pp. F1787-F1811, December 2018.
35. http://www.hsc.edu.kw/student/materials/course_notes/renal/index.htm, accessed April 2019.
36. Boston Scientific Corporation, Natick, MA, USA, https://www.bostonscientific.com/content/dam/bostonscientific/pi/portfolio-group/rfa/RFA-Family-Brochure-ENDO-149636-AA.pdf, accessed April 2019.
37. Y. MAESHIMA, H. MAKINO, *Angiogenesis and chronic kidney disease*, Fibrogenesis & Tissue Repair, **3**, *13*, pp. 1-17, 2010.
38. M. OSTEAUX, L. JEANMART, *Kidney tumor vascularization: morphology and angiogenesis, a microangiographic experimental study*, in: *Renal and adrenal tumors* (ed. E. Lohr), pp. 69-77, Springer, 1979.
39. BioDigital Inc., NY, USA, *Biodigital Human*, v. 3.1.3, 2017.
40. Dassault Systèmes, France, *Solidworks*, v. 2014.
41. S.S. SHIBESHI, W.E. COLLINS, *The rheology of blood flow in a branched arterial system*, Appl. Rheol., **15**, *6*, pp. 398-405, 2005.
42. Z. LIAO, C.K. POH, Z. HUANG, P.A. HARDY, W.R. CLARK, D. GAO, *A numerical and experimental study of mass transfer in the artificial kidney*, J. Biomech. Eng., **125**, *4*, pp. 472-480, 2003.
43. https://itis.swiss/virtual-population/tissue-properties/database/thermal-conductivity/, accessed April 2019.
44. D.F. PUTNAM, *Composition and concentrative properties of human urine*, Report, MCDonnell Douglas Astronautics Company – Western Division Huntington Beach, Calif. 92647 for Langley Research Center, National Aeronautics and Space Administration Washington, D.C., July 1971, https://ntrs.nasa.gov/archive/nasa/casi.ntrs.nasa.gov/19710023044.pdf
45. Comsol Inc., Sweden, *Comsol Multiphysics* (computer software), v.5.3a, 2018.
46. C.A. PERALTA, M.A. WHOOLEY, J.H. IX, M.G. SHLIPAK, *Kidney function and systolic blood pressure new insights from Cystatin C: Data from the heart and soul study*, Am. J. Hypertens., **1**9, *9*, pp. 939-946, 2006.

Received April 9, 2019